



HAL
open science

Multi-Spectroscopic Investigations for Comprehensive Structural Analysis of Aluminoborosilicate Glasses: II. Relation between the glass structure and chemical properties

Hanyu Hu, Sami Soudani, Jonathan Hamon, Nicolas Trcera, Michael Paris,
Yann Morizet

► To cite this version:

Hanyu Hu, Sami Soudani, Jonathan Hamon, Nicolas Trcera, Michael Paris, et al.. Multi-Spectroscopic Investigations for Comprehensive Structural Analysis of Aluminoborosilicate Glasses: II. Relation between the glass structure and chemical properties. *Glass Europe*, 2024, 2, pp.213-231. 10.52825/glass-europe.v2i.1424 . hal-04852456

HAL Id: hal-04852456

<https://hal.science/hal-04852456v1>

Submitted on 20 Dec 2024






HAL is a multi-disciplinary open access archive for the deposit and dissemination of scientific research documents, whether they are published or not. The documents may come from teaching and research institutions in France or abroad, or from public or private research centers.

L'archive ouverte pluridisciplinaire **HAL**, est destinée au dépôt et à la diffusion de documents scientifiques de niveau recherche, publiés ou non, émanant des établissements d'enseignement et de recherche français ou étrangers, des laboratoires publics ou privés.



Distributed under a Creative Commons Attribution 4.0 International License

Multi-Spectroscopic Investigations for Comprehensive Structural Analysis of Aluminoborosilicate Glasses: II. Relation between the glass structure and chemical properties

Hanyu Hu¹  <https://orcid.org/0009-0001-4961-3954>, Sami Soudani^{1,2}  <https://orcid.org/0009-0001-9301-2566>,
Jonathan Hamon¹, Nicolas Trcera³  <https://orcid.org/0000-0002-9364-1039>, Michael Paris¹  <https://orcid.org/0000-0002-8671-0630>,
and Yann Morizet^{1,2}  <https://orcid.org/0000-0001-9599-245X>

¹ Nantes Université, CNRS, Institut des Matériaux Jean Rouxel (IMN), 44322 Nantes Cedex, France

² Nantes Université, Nantes Atlantique Universités, Laboratoire de Planétologie et Géosciences de Nantes (LPG), UMR CNRS 6112, 44322 Nantes Cedex, France

³ Synchrotron SOLEIL, L'Orme des Merisiers, Départementale 128, 91190 Saint-Aubin, France

*Correspondence: Yann Morizet, yann.morizet@univ-nantes.fr

Abstract. Investigating how the chemical composition of glass influences its network structure is a crucial aspect in glass research. In this study, we have used the concept of glass optical basicity (Λ_{glass}), calculated from the chemical composition, to explore the relationship between the oxygen chemical environment and various structural parameters within complex network of Na- or/and Ca-bearing aluminoborosilicate glasses. We also incorporated extensive structural data from different glass systems reported in the literature. Our findings demonstrate a strong correlation between optical basicity and the following parameters: the maximum binding energy (B.E.) positions of the XPS O1s spectra, the chemical shifts of ²³Na and ²⁷Al from NMR spectra, the Ca-O distances from Ca K-edge XAS spectra, and the non-bridging oxygen (NBO) content calculated from ¹¹B and ²⁷Al NMR data. Furthermore, in low polymerization glasses, optical basicity also shows a strong correlation with the N_4 values (proportion of BO₄ species) obtained from ¹¹B NMR spectra and the apparent average n value of Qⁿ units derived from Raman spectra. The higher optical basicity aluminoborosilicate glasses is associated with higher oxygen binding energies, shorter Na-O and Ca-O distances, smaller Al-O-Si bond angles, higher NBO contents and lower degrees of network polymerization. This work provides new insights in using glass optical basicity for optimizing formulations of functional glasses and studying the effects of various components within glass systems.

Keywords: Aluminoborosilicate glasses, Structure of glass network, Glass optical basicity

1. Introduction

We outlined in Part I the existence of several key parameters to be used for characterizing glass structures, including network connectivity (average n value of Qⁿ units), non-bridging oxygen content (NBO%), and the role of cations, along with corresponding effective characterization methods: Raman spectroscopy, X-ray Photoelectron Spectroscopy (XPS), X-ray Absorption Spectroscopy (XAS) and Solid-State Nuclear Magnetic Resonance spectroscopy (NMR). In the present accompanying paper (Part II), we will delve into exploring the relationship between glass structure and chemical properties, aiming to explain the underlying reasons behind their correlation. Given the complexity of the glass system currently studied (CaO-Na₂O-Al₂O₃-B₂O₃-SiO₂), which encompasses various effects such as Mixed Former Effect (MFE, e.g. the RnKp series), Mixed Modifier Effect (MME, e.g. the CxNy series), and the influence of cation quantities (e.g. the RnKp and B15Nay series), the notions of R' and K' ($R' = ([\text{CaO}] + [\text{Na}_2\text{O}]) / ([\text{Al}_2\text{O}_3] + [\text{B}_2\text{O}_3])$, $K' = ([\text{SiO}_2]) / ([\text{Al}_2\text{O}_3] + [\text{B}_2\text{O}_3])$) used in Part I appear insufficient for discussing such a broad range of compositions in different

glass systems. For instance, the model developed by Dell et al. [1] and the subsequent improvement made by Du and Stebbins [2] addressed the structural changes involved in Na-bearing glass series and so far; these models have not yet been adapted to analyze Ca-bearing aluminoborosilicate glasses. Only the model of Dell modified by Lu et al. [3], has incorporated Ca by introducing a coefficient of glass modifier a_i with the help of machine learning. However, the rationale behind this coefficient remains unverified. Alternatively, it is crucial to select an appropriate representative parameter for chemical properties to compare effectively all the investigated glasses.

In diverse applications of complex silicate glasses and slags, such as metallurgical extraction, nuclear waste immobilization, and geochemistry, the concept of “basicity” finds extensive application in oxide studies. Historically, in the molten glass state, the bonding between oxides was interpreted as an acid (covalent network oxide) – base (ionic oxide) reaction. However, due to the challenge of measuring single ion activity, the application range of parameter like potential values, akin to solution pH values, is limited. This limitation arises from the inability to compare, for example, Na-bearing silicate melt with Ca-bearing silicate melt [4]. Additionally, basicity has been used to quantify the activity of free oxygen ions (i.e. O^{2-}). For example, studies have examined the dependency of refractive index and absorption coefficient on basicity in Ca, Mg, and Al-bearing silicate slag [5], and investigated the influence of compositions in Ti_2O_3 -doped silicate, borate and phosphate glasses on the Ti^{3+}/Ti^{4+} oxidation-reduction reaction [6].

Another widely acknowledged concept is the optical basicity (Λ_{glass}), initially proposed in the 1970s by Duffy and Ingram [7,8]. Originally, Λ_{glass} was measured by introducing trace metal ions, such as Tl^+ , Pb^{2+} and Bi^{3+} , during glass melting, using UV probe spectroscopy to quantify the negative charge donating ability of oxygen atoms, known as the nephelauxetic effect. Subsequently, more studies have measured Λ_{glass} using alternative methods, including electron density [9], electronegativity (Λ_{XAV}) [10,11], energy gap (Λ_{EG}) [11,12], refractive index (Λ_n) [13,14], and ionic-covalent parameters (Λ_{ICP}) [15,16]. Moreover, Λ_{glass} has demonstrated strong predictive capabilities in transport properties, including viscosity, electrical conductivity, and diffusion [17]. Additionally, it is also correlated with thermochemical properties such as entropy of fusion, thermal expansion coefficient and thermodynamic activity coefficients [17–19], as well as properties like magnetism [20], catalysis [21,22], and lubrication [23]. In terms of glass structure, Λ_{glass} has been shown to be closely related to the non-bridging oxygen per tetrahedron (NBO/T) [17] and the band energy of XPS O 1s peak [24], representing the overall average state of oxygen in the glass network. Λ_{glass} has been validated not only in relation to the physical properties of glass but also as a predictive tool for the structure of functional glasses. For example, it has also been used to explain the tendency for nepheline ($NaAlSiO_4$) crystallization in high-level radioactive waste vitrification glasses [25].

Nonetheless, many additional aspects related to the glass optical basicity are to be explored. For instance, recent work [26] has shown that Λ_{glass} could be used to predict iodine solubility in aluminoborosilicate glasses synthesized under high-pressure conditions. However, the proposed work suffered from approximation in the calculation of the Λ_{glass} considering that the effect of pressure on the glass structure was not determined. The work of Soudani et al. [27] showed that B speciation is strongly affected by pressure conditions. According to Dimitrov et al. [28], the change in the network forming elements and their associated structural units (i.e. Q^n species for Si, aluminate species and borate species) should be taken into account for calculating a reliable value for glass optical basicity. Applying the concept of glass optical basicity could also be beneficial for other volatile elements modelling such as CO_2 or SO_2 in silicate glasses [29–31] owing to the fact that their dissolution mechanisms have been found to be controlled by oxygen speciation (i.e. BO and NBO distribution in glasses).

In the present work, we wish to capitalize on the various knowledge that we acquired on the structure of aluminoborosilicate glasses as demonstrated in the Part I of the accompanying paper. We propose to discuss the combination between the theoretical Λ_{glass} values, determined from the glass chemical composition, and experimentally obtained structural information of glass. Our objectives include verifying whether Λ_{glass} can still serve as a reliable reference for the oxygen chemical environment in complex aluminoborosilicate glass systems and exploring the impact of the oxygen chemical environment on the other atoms within the glass network.

2. Methods for the calculation of the glass optical basicity

The theoretical glass optical basicity Λ_{Glass} was calculated according to the equation of Duffy based on the compositions of oxide systems [8]:

$$\Lambda_{\text{Glass}} = \sum \frac{X_i}{\gamma_i} = \sum X_i \times \Lambda_i \quad (1)$$

Where X_i represents the oxygen molar fraction of the oxide i , and γ_i represents the basicity moderating parameters of the oxide i . For all the glasses, the value of γ_i or Λ_i ($1/\gamma_i$) referred to the work of Rodriguez et al. [25]. The calculated Λ_{Glass} for investigated glasses is reported in Table 1. We used the glass chemical composition determined by SEM EDS (B_2O_3 is determined using LA-ICP-MS, see Part I) or reported in subsequent publications [32,33]. It is worth emphasizing that the calculated Λ_{Glass} represents an approximate value of the glass optical basicity, not the value measured by experimental methods as mentioned previously.

In the present calculation of the Λ_{Glass} we did not consider the distribution of the structural species as suggested in Dimitrov et al. [28]. As such, it would require investigating the glass speciation for obtaining the distribution between BO_3 and BO_4 for the borate network; the distribution between AlO_4 , AlO_5 and AlO_6 for the aluminate network; and the Q^n species distribution of the silicate network, in which the Q^n species represents a silicon tetrahedral unit with n BOs. Whereas the B and Al species distributions have been extracted from the NMR analyses we have conducted, the Q^n species distribution cannot be accessed in a quantitative way considering that we do not have performed ^{29}Si NMR investigation. Moreover, one of the objectives is to determine if the relationships between a simple calculation from glass chemical composition and advanced structural probing exist.

Nonetheless, we have tested the change in the Λ_{Glass} if the distribution of B and Al species is considered. For doing so, we have taken the γ_{BO_3} and γ_{BO_4} provided by Dimitrov et al. [28]: 2.38 and 4.17, respectively. For C0N35 (see Table 1) that is the glass with the highest B_2O_3 content (~30 mol.%), the N_4 value is 0.53, which corresponds to absolute number of 14.4 and 16.3 mol. for BO_3 and BO_4 , respectively; the Λ_{Glass} is decreased by 0.034 between 0.555 and 0.521. This is the most important change in Λ_{Glass} observed and it does not exceed 10% in relative to the value. For Al species, the main problem is that there is currently no existing γ values for AlO_5 species. Komatsu et al. [34] reported γ_{AlO_4} and γ_{AlO_6} values: 1.67 and 2.5, respectively. We can expect the γ_{AlO_5} value to be intermediate in between the two. At first sight, we might speculate on a non-negligible change in the Λ_{Glass} owing to the large change in γ , however, the total Al_2O_3 content in our glass does not exceed 7.2 mol.% in Ca-R2K1 glass. For this glass, the Al species distribution is 80.9% and 19.1% for AlO_4 and AlO_5 species and no AlO_6 . It corresponds to absolute number of 5.8 and 1.4 mol. for AlO_4 and AlO_5 , respectively. Considering an intermediate value for γ_{AlO_5} of 2.09 and integrating the change in B speciation, we have calculated a change in the Λ_{Glass} of 0.010 between 0.596 and 0.586. This change in the Λ_{Glass} is negligible and we will only consider the Λ_{Glass} calculated from glass chemical composition without taking into account the element speciation.

Table 1. Calculated optical basicity and key parameters of network structure of investigated glasses along with corresponding characterization methods, including the R' value ($([Na_2O] + [CaO])/([Al_2O_3] + [B_2O_3])$), the band energy of maximum intensity of XPS O 1s peak (B.E.max, ± 0.2 eV), the isotropic chemical shift of sodium and 4-fold coordinated aluminum (δ_{Na} , $\delta_{[4]Al}$, ± 0.3 ppm), the quadrupolar coupling constant of sodium and 4-fold coordinated aluminum (CQ_{Na} , $CQ_{[4]Al}$, ± 0.2 MHz), Ca-O distance (r_{Ca-O} , Å), NBO content (NBO%), proportion of 4-fold coordinated borate species (N_4) and apparent average Q^n value (Appa. Q^n). The error bars are reported in between brackets and were estimated by the propagation of uncertainty or estimated from the spectra fitting processes.

Glass ID	Λ_{Glass}^*	R'	B.E.max O 1s	δ_{Na} (NMR)	CQ_{Na} (NMR)	$\delta_{[4]Al}$ (NMR)	$CQ_{[4]Al}$ (NMR)	rCa-O (XAS)	NBO% (NMR)	N_4 (NMR)	Appa. Q^n (Raman)
CaNa-R2K1	0.650	2.8	531.5	6.5	3.2	67.3	5.0	2.55(28)	50.4(5)	0.17(6)	2.7(1)
CaNa-R2K2	0.597	2.6	532.0	1.0	3.2	64.8	5.1	2.66(32)	31.7(4)	0.40(6)	3.1(1)
CaNa-R2K3	0.565	2.2	532.2	-3.2	3.0	63.0	5.3	2.67(32)	21.8(3)	0.52(6)	3.3(1)
CaNa-R3K2	0.631	3.2	531.7	6.0	3.3	66.7	4.9	2.54(28)	45.7(4)	0.22(6)	2.8(1)
CaNa-R3K3	0.611	3.6	532.1	2.6	3.3	65.2	5.1	2.60(29)	39.1(3)	0.39(6)	3.1(1)
CaNa-R3K4	0.584	3.2	532.6	-0.5	3.2	63.7	5.1	2.66(66)	29.4(3)	0.51(6)	3.3(1)
Ca-R2K1	0.595	1.7	531.5	-	-	66.3	6.6	2.59(28)	37.2(7)	0.21(6)	2.8(1)
Ca-R2K2	0.564	1.6	531.5	-	-	63.4	6.9	2.65(27)	25.4(5)	0.27(6)	3.0(1)
Ca-R2K3	0.545	1.5	531.9	-	-	62.7	6.9	2.68(68)	17.5(4)	0.24(6)	3.0(1)
Ca-R3K2	0.602	2.5	531.6	-	-	65.9	6.6	2.54(54)	41.9(5)	0.24(6)	2.8(1)
Ca-R3K3	0.581	2.5	531.8	-	-	63.9	6.8	2.57(57)	34.0(4)	0.26(6)	3.0(1)
Ca-R3K4	0.562	2.3	532.0	-	-	63.1	6.8	2.66(30)	27.3(3)	0.24(6)	3.1(1)
C35N0	0.542	1.0	n.a.	-	-	62.8	6.1	n.a.**	19.1(9)	0.33(6)	2.9(1)
C30N5	0.543	1.0	n.a.	-7.7	2.6	62.9	5.7	n.a.	17.6(9)	0.35(6)	3.0(1)
C20N15	0.546	1.0	n.a.	-3.6	2.9	63.9	4.9	n.a.	15.2(9)	0.41(6)	3.1(1)
C10N25	0.551	0.9	n.a.	-0.6	3.1	64.6	4.8	n.a.	14.5(9)	0.44(6)	3.2(1)
C0N35	0.555	0.9	n.a.	1.3	3.2	64.9	4.6	n.a.	10.7(9)	0.53(6)	3.4(1)
B15Na10	0.504	0.5	532.3	-12.4	2.5	59.2	5.1	n.a.	0.0	0.36(6)	3.7(1)
B15Na20	0.526	0.9	531.7	-6.5	2.8	61.8	5.2	n.a.	3.8(4)	0.65(6)	3.5(1)
B15Na30	0.565	1.4	531.5	-0.5	2.9	63.7	5.0	n.a.	15.4(5)	0.61(6)	3.4(1)
B15Na40	0.594	1.7	531.2	3.4	2.7	65.8	4.5	n.a.	25.1(5)	0.37(6)	3.0(1)

*: optical basicity values are calculated by Eq 1.

**.: not analyzed.

3. Results and discussion

3.1 Chemical environment of oxygen

As mentioned in Part I, the chemical environment of oxygen can be directly measured by XPS since the changes in the electron density within the valence band of an oxygen affects the energy with which electrons are bound to the oxygen nucleus, therefore affecting the binding energy (B.E.). While, the Λ_{Glass} can represent the overall average state of oxygen in glass. Previous works have observed a negative correlation between B.E. of O 1s peak obtained by XPS and the calculated Λ_{Glass} in simple glass systems like $\text{Na}_2\text{O-SiO}_2$ [24,35] and $\text{Na}_2\text{O-B}_2\text{O}_3\text{-SiO}_2$ [36]. In Figure 1, we show the change in B.E. O 1s determined for the investigated $\text{CaO-Na}_2\text{O- Al}_2\text{O}_3\text{-B}_2\text{O}_3\text{-SiO}_2$ glasses (see Table 1) as function of Λ_{Glass} along with the data from the literature: $\text{Na}_2\text{O-SiO}_2$ from Matsumoto et al. [24] and Nesbitt et al. [35]; $\text{Na}_2\text{O-B}_2\text{O}_3\text{-SiO}_2$ from Miura et al. [36]. The literature data focuses on relatively simple glass systems for which the distinction between BO and NBO is much easier. In the literature data, they give a clear distinction between the NBO and BO peaks in the XPS O 1s spectra and all the points correspond to the B.E. obtained for the O_{BO} 1s peak. Variations in B.E. for the O_{NBO} 1s follow a similar trend with a lower B.E. value. For our investigated glasses, considering that, the NBO and BO peaks strongly overlap; the B.E. values reported in Figure 1 correspond to the O 1s peak at maximum intensity. From the Figure 1, we observe that glasses with the same Λ_{Glass} can exhibit different B.E. values, glasses showing the same B.E. can exhibit different Λ_{Glass} value. Glasses with a Λ_{Glass} value of approximately 0.6, such as CaNa-R2K2, CaNa-R3K3, Ca-R2K2, Ca-R3K3, and B15Na40 glasses, have B.E. values of 532.1, 532.0, 531.6, 531.5, and 531.2 eV, respectively. However, when examining each series, the B.E. values shift towards lower energy with increasing Λ_{Glass} . This trend is consistent with the literature data in which, the negative slope is nearly identical: a decrease in B.E. of ~ 0.5 eV corresponds to an increase in the Λ_{Glass} value of ~ 0.05 . It corroborates the strong correlation between O 1s B.E. values and Λ_{Glass} . Other factors influencing B.E. values include the complexity of the glass system. For example, the B.E. values in the $\text{Na}_2\text{O-B}_2\text{O}_3\text{-SiO}_2$ system are lower than those in the $\text{Na}_2\text{O-SiO}_2$ system with same Λ_{Glass} values. The type of modifying cation (i.e. Na^+ , Ca^{2+} or both) also affects B.E. values, for example, CaNa-R2Kp and CaNa-R3Kp glass series have higher B.E. values than Ca-R2Kp and Ca-R3Kp glass series for a given Λ_{Glass} value, with a difference of around 1 eV (see Figure 1). Additionally, the R' value of the studied system might play a role, owing to the fact that CaNa-R2Kp and Ca-R2Kp glass series have higher B.E. values as compared to CaNa-R3Kp and Ca-R3Kp glass series with same Λ_{Glass} values. However, the difference appears small (~ 0.25 eV), and possibly within the error of the XPS determination. It is worth emphasizing that even for the same $\text{Na}_2\text{O-SiO}_2$ system in the literature (Matsumoto et al. [24] and Nesbitt et al. [35]), identical compositions can yield different B.E. values, likely due to experimental errors, as the trends of the two lines are completely consistent.

By verifying the relationship between Λ_{Glass} and B.E. of O 1s, we can establish that the calculated Λ_{Glass} value, a parameter solely derived from the chemical composition of glass, is indeed closely related to the overall chemical environment of oxygen in the glass network. It highlights the potential of using XPS to study the impact of compositional variations within the same glass system on the oxygen environment. This approach provides a valuable tool for understanding how changes in specific components affect the overall glass structure. By extension, the observed linear relationship between O 1s B.E. (i.e. oxygen environments) and Λ_{Glass} value also suggests that Λ_{Glass} value could be used for correlation with other variables such as volatile element solubility and speciation. Recently, Morizet et al. [33] related the iodine dissolution mechanisms with the nature of oxygen atoms. Previous works showed that C and S dissolutions as CO_3^{2-} and SO_4^{2-} , respectively; were strongly correlated to the distribution between BO and NBO atoms [29,31,37–39]. It would be pertinent to observe a potential correlation between CO_2 and S solubilities with Λ_{Glass} .

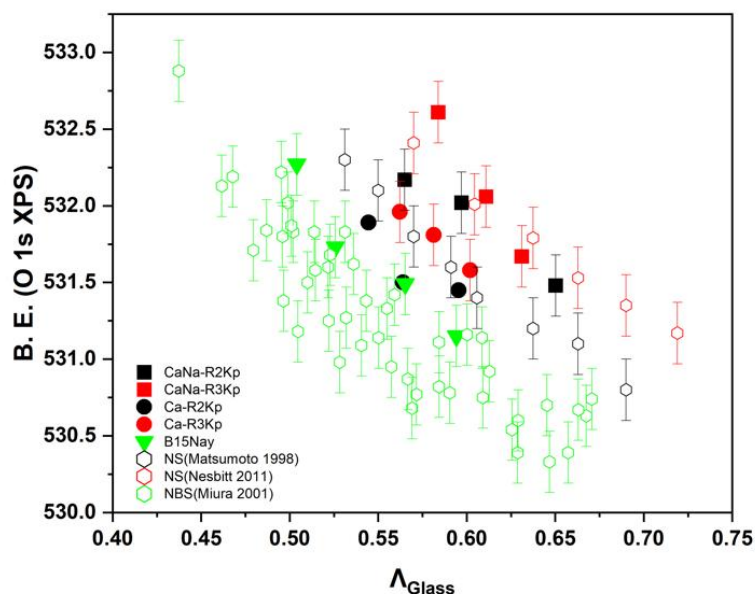


Figure 1. Evolution of B.E. of O 1s XPS peak as function of Λ_{glass} . Data from this study (solid points) were obtained by measuring the maximum intensity of the O 1s peak. Literature data (open points) correspond to the band energy of the BO O 1s peak. Error bars are set at ± 0.2 eV, as reported in the literature.

3.2 Chemical environment of sodium and calcium

The local environment of sodium in the glass samples is characterized by ^{23}Na NMR, focusing on the isotropic chemical shift (δ_{Na}) and the quadrupolar coupling constant (CQ_{Na}). The relationship between Λ_{Glass} and these two parameters is reported in Figure 2A and Figure 2B, respectively. In Figure 2A, the solid points represent the results from our investigated glasses, the open squares represent previously published results by our group, and other open symbols represent results from similar glass systems reported in the literature.

The Figure 2A shows that, for most data points, the δ_{Na} value increases with increasing Λ_{Glass} value. For example, the data points for CaNa-RnKp and B15Nay glass series show an almost linear increase, with Λ_{Glass} increasing from 0.50 to 0.65 and the δ_{Na} increasing from -12.4 to 6.5 ppm. However, other compositional parameters also influence the chemical shift of ^{23}Na . Firstly, as reported by Bradmüller et al. [40], the Al/B ratio, represented by the composition line $60\text{SiO}_2-x\text{Al}_2\text{O}_3-(20-x)\text{B}_2\text{O}_3-20\text{Na}_2\text{O}$, affects δ_{Na} . The corresponding four data points in Figure 2A have x values of 5, 10, 15 and 20 from left to right as marked by the red arrow (Al/B ratio) in Figure 2A. Although Λ_{Glass} increases with the replacement of B_2O_3 by Al_2O_3 , the δ_{Na} remains constant. Secondly, the Mixed Modifier Effect (MME) on the δ_{Na} is also apparent. For instance, in the CxNy series and in two $\text{CaO-Na}_2\text{O-Al}_2\text{O}_3-\text{B}_2\text{O}_3-\text{SiO}_2$ series from Wu et al. [41], Ca progressively replaces Na in the glass ($x\text{Na} = \text{Na}_2\text{O}/(\text{Na}_2\text{O}+\text{CaO})$, while other component concentrations remain unchanged), the Λ_{Glass} values are around 0.55. As xNa increases marked by the blue arrow in the Figure 2A, the δ_{Na} increases from -10 to 1 ppm. The glasses in our study show the same trend as those in the literature (black triangles), indicating that the δ_{Na} is indeed influenced by MME. Thirdly, the ratio Al/Si also has an impact on δ_{Na} as indicated by data from Zheng et al. [42] with the composition line $(80-x)\text{SiO}_2-x\text{Al}_2\text{O}_3-5\text{B}_2\text{O}_3-15\text{Na}_2\text{O}$ marked by the black arrow (Al/Si ratio). With increasing replacement of SiO_2 by Al_2O_3 , Λ_{Glass} rises from 0.52 to 0.55, which δ_{Na} dramatically decreases from 2 to -12 ppm.

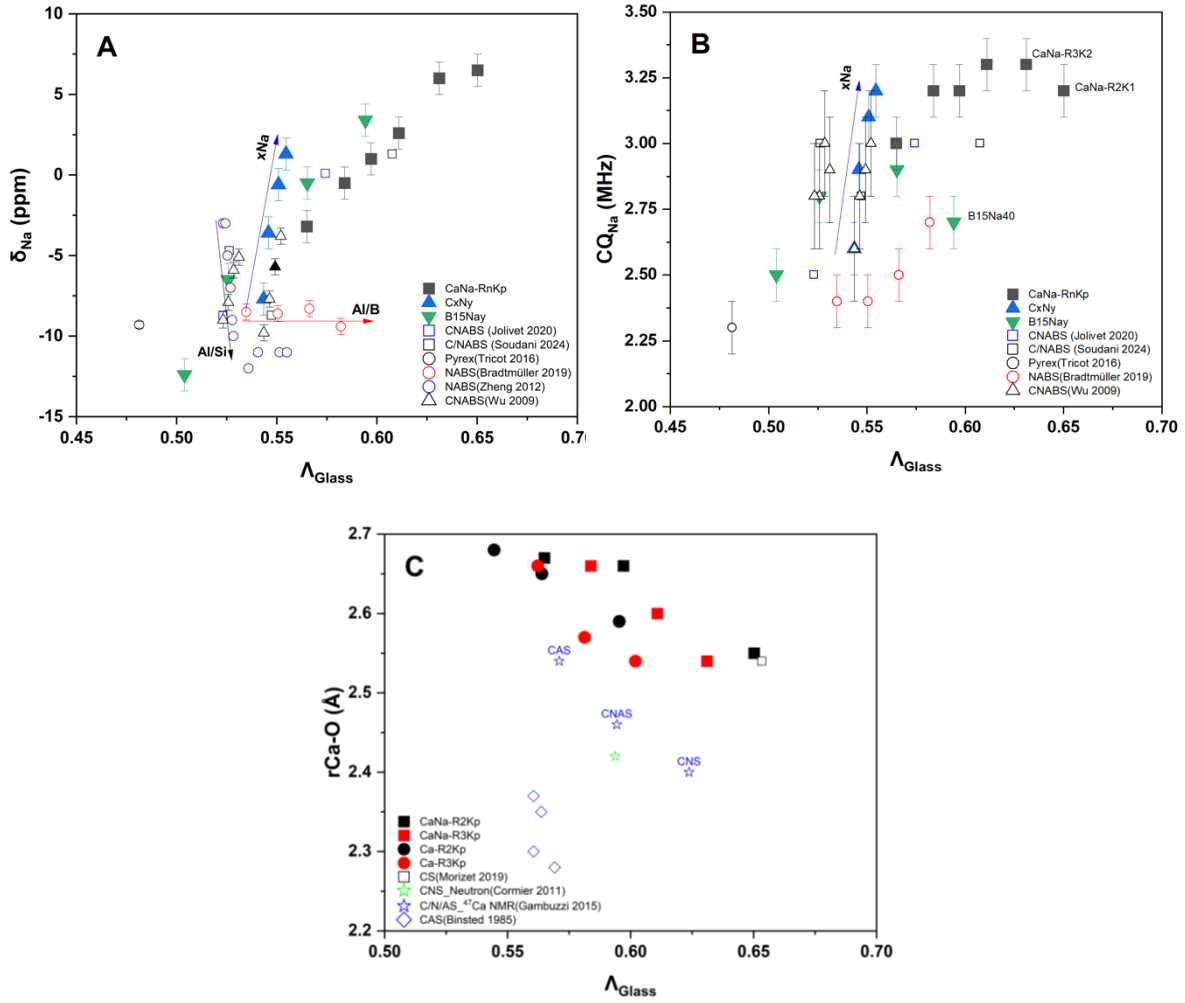


Figure 2. Evolution of isotropic chemical shift (A) and quadrupolar coupling constant (B) of ^{23}Na derived from ^{23}Na NMR spectra and Ca-O distance derived from Ca K-edge XAS spectra (C) as function of Λ_{glass} . The solid points are standing for the investigated glasses in this study and the open points are standing for the data reported in the literature. In Figure 2A, blue, red and black arrows indicate the increase xNa (CxNy series and series reported in Wu et al., 2009^[41]), Al/B ratio (series reported in Bradtmüller et al., 2019 [40]), and Al/Si ratio (series reported in Zheng et al., 2012 [42]), respectively. The blue arrow in Figure 2B indicates the same as the blue arrow in Figure 2A. Error bars for δ_{Na} and CN_{Na} are ± 1 ppm and ± 0.2 MHz for our glasses, respectively, with values from the literature used for others. The error for $r_{\text{Ca-O}}$ is approximately 0.3 Å, as provided by the fit software Artemis (not shown).

As previously mentioned in Part I, δ_{Na} is sensitive to the average Na-O distance ($d_{\text{Na-O}}$). Several studies have observed that δ_{Na} increases as $d_{\text{Na-O}}$ decreases [43–46]. Empirical relationships between these two parameters have been proposed based on the crystalline silicates, aluminosilicate compounds [45,47,48] as well as glasses [49]. Since the role of sodium in network is related to the $d_{\text{Na-O}}$, numerous studies have demonstrated that Na-modifiers are located near NBOs, while Na-charge compensators are positioned in the vicinity of tetrahedral BO_4 or AlO_4 units to balance the excess negative charge. Under those circumstances, the Na-charge compensators exhibit longer $d_{\text{Na-O}}$. Accordingly, as shown in Figure 2A, Na increasingly acts as a modifier with the general increases of Λ_{glass} . A particularly noteworthy result is the pronounced MME illustrated in Figure 2A. When Na is replaced by Ca, the theoretical Λ_{glass} remains relatively constant, while δ_{Na} shows a marked decrease. This suggests that in Ca-rich aluminoborosilicate glasses, Na initially tends to act more as a compensator. Meanwhile, the MFE of Al/B reals that substituting B_2O_3 with Al_2O_3 has minimal impact on the primary role of Na, as equal amounts of tetrahedral BO_4 or AlO_4 units necessitate an equivalent amount of Na to serve as charge compensator. For the MEF

of Al/Si shows that replacing SiO₂ with Al₂O₃ significantly changes the role of Na from modifier to charge compensator. This observation introduces a novel approach for studying, even comparing the impact of compositional parameters, using Λ_{glass} as a reference.

Although CQ_{Na} is not as useful as δ_{Na} as a local probe for $d_{\text{Na-O}}$ and coordination number due to its sensitivity to local sites distortions [48], it is still interesting that CQ_{Na} exhibits systematic changes with composition. As shown in Figure 2B, for Na₂O-Al₂O₃-B₂O₃-SiO₂ and CaO-Na₂O-Al₂O₃-B₂O₃-SiO₂ glasses, CQ_{Na} increases from 2.25 (Pyrex[®] [50]) to 3.25 MHz with increasing Λ_{glass} . The trend is evident across B15Nay and CaNa-RnKp series. Besides, the MME is evident in the CxNy series and previously reported CaO-Na₂O-Al₂O₃-B₂O₃-SiO₂ glasses (Wu et al. [41]), where CQ_{Na} rises with Na content. The increase of CQ_{Na} may due to the change in the coordination number (CN) from 6 to 5 as described in the literature: CN = 6, triangular prism, $CQ_{\text{Na}} \approx 2.0$ MHz; CN = 5, square pyramid, $CQ_{\text{Na}} \approx 2.8$ MHz [48]. For glasses with CQ_{Na} exceeding 2.8 MHz, this can be attributed to the rising proportion of Na⁺ cation near NBO (Na-modifier) for which the electric field gradient (EFG) is higher than for the ones close to BO (Na-charge compensator).

The Ca chemical environment in the glass samples has been characterized by Ca K-edge X-ray Absorption Spectroscopy (XAS, see Part I), specifically through the determination of the distance between Ca²⁺ and the first nearest neighbour oxygen ($r_{\text{Ca-O}}$) and also the coordination number between Ca atoms and surrounding O atoms ($CN_{\text{Ca-O}}$). There are relatively few studies using Ca K-edge XAS to obtain $r_{\text{Ca-O}}$ in glass materials, such as in CaO-SiO₂ [52] and CaO-Al₂O₃-SiO₂ [52–55] systems. Other methods have been used to study the chemical environment of calcium, including neutron diffraction [56,57], molecular dynamic simulation [58], an ⁴³Ca NMR [59,60]. In the current work, we have tried to compile and compare our results with available literature data. However, we excluded the studies by Hannon et al. [56] and Cormier et al. [58] from the comparison because their focus was on CaO-Al₂O₃ and CaO-Al₂O₃-SiO₂ glass systems, with very high Al₂O₃ content and even higher than SiO₂ content in the glass. It significantly differs from our glass compositions and comparison might be unreliable. The relationship between Λ_{glass} and $r_{\text{Ca-O}}$ is reported in Figure 2C.

The Figure 2C shows that in our investigated glasses, $r_{\text{Ca-O}}$ decreases with increasing Λ_{glass} . Although the data points are limited, this trend appears nearly linear in the CaNa-R2Kp, CaNa-R3Kp, Ca-R2Kp and Ca-R3Kp series, with each series exhibiting approximately a 0.1 Å change. Despite this difference falling within the error range of XAS measurements, the consistent trend across all four glass series suggests the presence of a relevant correlation in between the glass optical basicity and the local environment of Ca in glasses. Additionally, similar trends are observed in the ⁴³Ca NMR fitted data [59] for CaO-Al₂O₃-SiO₂, CaO-Na₂O-Al₂O₃-SiO₂, and CaO-Na₂O-SiO₂ glasses (showing a change of about 0.15 Å) and in the XAS results [53] for CaO-Al₂O₃-SiO₂ systems (showing a change of about 0.1 Å), with corresponding Λ_{glass} values calculated using Eq. 1. This further supports the reliability of the observed relationship between Λ_{glass} and $r_{\text{Ca-O}}$. It is noteworthy that the $r_{\text{Ca-O}}$ values we obtained (mean value of 2.6 Å) differ significantly from those reported in the literature (mean values of 2.45 and 2.3 Å). This discrepancy might be due to differences in the investigated glass systems, as our studied glasses contain relatively higher B₂O₃ contents. It could be due to experimental errors or the way the simulation of the Ca EXAFS radial distribution function is carried out that is strongly model dependent. Due to the limited amount of available data and the lack of references, it is challenging to determine the exact cause of this discrepancy.

In summary, the ²³Na NMR and Ca XAS data both indicate that the chemical environments of Na and Ca are closely related to the overall oxygen chemical environment in the glass. For high Λ_{glass} value (i.e. indicating high oxygen activity), the distances between Na and O, as well as Ca and O, are relatively shorter. Although it was expected, this relationship underscores the significant influence of oxygen activity on the positioning and behaviour of these cations within the glass network.

3.3 Chemical environment of aluminium

The chemical environment of aluminium in the glass samples has been characterized by ^{27}Al NMR, including the isotropic chemical shift ($\delta_{[4]\text{Al}}$) and the quadrupolar coupling constant ($\text{CQ}_{[4]\text{Al}}$). We focused our attention to the 4-fold coordinated Al species considering that it is the most abundant species observed in the investigated glasses. The relationship between the Λ_{glass} and these two parameters is shown in Figure 3A and 3B, respectively. We also provide results from previously published data from similar glass systems reported in the literature.

The Figure 3A demonstrates a strong positive linear correlation between $\delta_{[4]\text{Al}}$ and Λ_{glass} , applicable to both our investigated glasses and to those reported in the literature [40,42,50,61–66]. For instance, the Pyrex[®] glass [50], which has the lowest Λ_{glass} value of 0.48, shows a $\delta_{[4]\text{Al}}$ of 56.5 ppm, whereas the CaNa-R2K1 glass, which has the highest Λ_{glass} value of 0.65, exhibits a $\delta_{[4]\text{Al}}$ of 67.3 ppm. This significant range indicates a robust relationship between $\delta_{[4]\text{Al}}$ and Λ_{glass} . Furthermore, this correlation appears consistent across different glass systems, as $\text{Na}_2\text{O}-\text{Al}_2\text{O}_3-\text{SiO}_2$ [61], $\text{CaO}-\text{Al}_2\text{O}_3-\text{SiO}_2$ [61,65,66], $\text{Na}_2\text{O}-\text{Al}_2\text{O}_3-\text{B}_2\text{O}_3-\text{SiO}_2$ [40,64], $\text{CaO}-\text{Al}_2\text{O}_3-\text{B}_2\text{O}_3-\text{SiO}_2$ [27] and $\text{CaO}-\text{Na}_2\text{O}-\text{Al}_2\text{O}_3-\text{B}_2\text{O}_3-\text{SiO}_2$ [50] glasses all follow the same correlation line. Notably, in our investigated glasses, the Al/Si ratio is consistently less than 1. As a result, data from $\text{CaO}-\text{Al}_2\text{O}_3-\text{SiO}_2$ glasses with Al/Si > 1, reported by Neuville et al. [66] were excluded, even though this positive correlation can also be observed in high- Al_2O_3 aluminosilicate glasses.

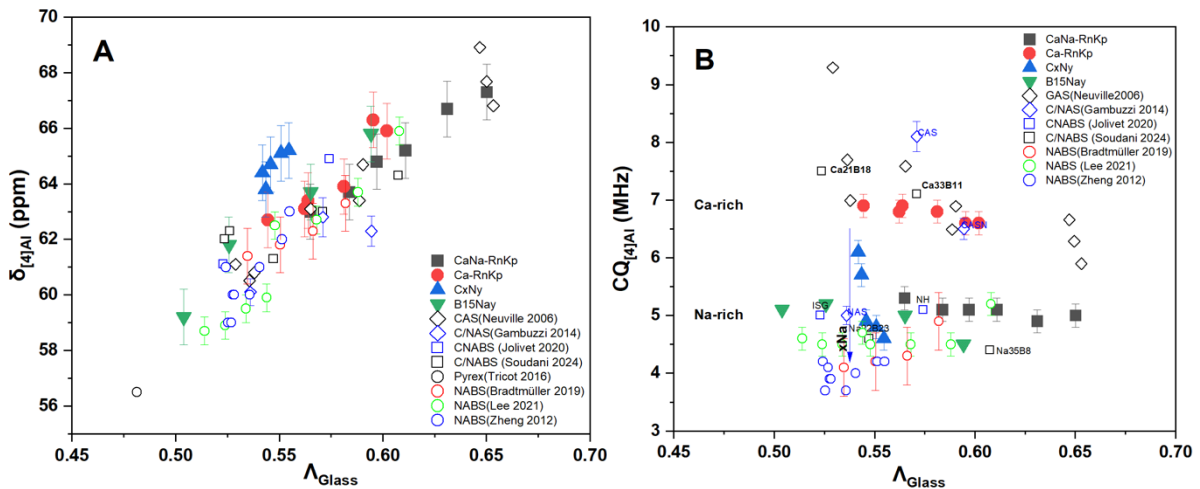


Figure 3. Evolution of isotropic chemical shift (A) and quadrupolar coupling constant (B) of ^{27}Al for 4-fold coordinated Al species derived from ^{27}Al NMR spectra, as function of Λ_{glass} . Solid points indicate the investigated glasses in this study, while open points correspond to data from the literature. In Figure 3B, the blue arrow indicates the increase in xNa within the C_xN_y series. The error bars for δ_{Al} and $\text{CQ}_{[4]\text{Al}}$ in our investigated glasses are ± 1 ppm and ± 0.2 MHz, respectively. Error bars for other glasses are as reported in the literature.

Based on previous ^{27}Al NMR studies reported in the literature, the δ_{Al} is primarily related to the degree of coordination of Al atoms (i.e. $\delta_{[4]\text{Al}} \approx 60$ ppm, $\delta_{[5]\text{Al}} \approx 30$ ppm, $\delta_{[6]\text{Al}} \approx 0$ ppm). However, another important factor affecting the δ_{Al} value is the Al-O-Si bond angle. A negative correlation between these two parameters has been observed both in crystalline aluminosilicate compounds [67–69] and in aluminosilicate glasses [65,70,71]. In addition, Angeli et al. [72] proposed that the continuous decrease in the Al-O-Si angle is attributed to the continuous decrease in the distance between $\text{M}^{\text{n+}}-\text{O}$ in $\text{CaO}-\text{Al}_2\text{O}_3-\text{B}_2\text{O}_3-\text{SiO}_2$ glasses. This is because the T-O-T triplets are increasingly disturbed by the presence of the modifiers in the immediate surrounding. Those findings align with our observations in the previous sections, where we suggest that as Λ_{glass} increases, the $d_{\text{Na-O}}$, $r_{\text{Ca-O}}$ and Al-O-Si bond angle

decrease, supported by chemical shift of ^{23}Na , Ca K-edge XAS analysis and ^{27}Al chemical shift of AlO_4 species, respectively.

The Figure 3B suggests that the $\text{CQ}_{[4]\text{Al}}$ value is independent with the Λ_{glass} value. However, two regions can be identified: the $\text{CQ}_{[4]\text{Al}}$ is notably higher in Ca-rich aluminoborosilicate glasses compared to Na-rich ones. For instance, in $\text{Na}_2\text{O}-\text{Al}_2\text{O}_3-\text{SiO}_2$ glass, such as the NAS glass reported by Gambuzzi et al. [61], in $\text{Na}_2\text{O}-\text{Al}_2\text{O}_3-\text{B}_2\text{O}_3-\text{SiO}_2$ glasses, such as the B15Nay series, C0N35 glass, and data from Bradtmüller et al. [40], Lee et al. [64], and Soudani et al. (Na22B23 and Na35B8 glasses) [63], as well as in $\text{Na}_2\text{O}-\text{CaO}-\text{Al}_2\text{O}_3-\text{B}_2\text{O}_3-\text{SiO}_2$ glasses with $x_{\text{Na}} > 0.4$, including the C10N25 and C20N15 glasses in the CxNy series, the CaNa-RnKp series, ISG [62] and NH [62] glasses, $\text{CQ}_{[4]\text{Al}}$ values range between 3.5 and 5.5 MHz. In contrast, in $\text{CaO}-\text{Al}_2\text{O}_3-\text{SiO}_2$ glasses, such as data from Neuville et al. [66] and the CAS glass reported by Gambuzzi et al. [61], in $\text{Na}_2\text{O}-\text{CaO}-\text{Al}_2\text{O}_3-\text{B}_2\text{O}_3-\text{SiO}_2$ glasses with $x_{\text{Na}} < 0.4$, such as the C30N5 glass and the CASN glass reported by Gambuzzi et al. [61], as well as in $\text{CaO}-\text{Al}_2\text{O}_3-\text{B}_2\text{O}_3-\text{SiO}_2$ glasses like the Ca-RnKp series, C35N0 glass, Ca21B18 and Ca33B11 glasses in Soudani et al. [63], $\text{CQ}_{[4]\text{Al}}$ values are higher, range from 5.5 to 9.3 MHz. This difference is also evident by examining the MME in CxNy series, where a decrease in x_{Na} associated with a significant increase in $\text{CQ}_{[4]\text{Al}}$ ($\Delta\text{CQ}_{[4]\text{Al}} = 1.5$ MHz), highlighting the impact of Ca content on $\text{CQ}_{[4]\text{Al}}$. This can be explained by the fact that the proximity of high-field-strength Ca^{2+} cations near the Al species induces a distortion in the AlO_4 tetrahedron units, deviating them from tetrahedral symmetry. Consequently, Figure 3B underscores the substantial impact of Na or Ca as charge compensators on $\text{CQ}_{[4]\text{Al}}$ of AlO_4 species: in Na-rich aluminoborosilicate glasses, sufficient Na content allows Na to preferentially charge compensate AlO_4 species, resulting in relatively lower $\text{CQ}_{[4]\text{Al}}$ values. When Ca assumes the role of charge compensator for AlO_4 species, the $\text{CQ}_{[4]\text{Al}}$ increases substantially. This phenomenon has also been reported in the studies of ZrO_2 and rare-earths (Nd, La)-bearing soda lime aluminoborosilicate glasses [73].

3.4 Degree of polymerization

To address the degree of polymerization of glass network, the average Q^n provides a direct view of the global structure of the silicate network. According to the model of Dell et al. [1], the N_4 value can also indicate the polymerization process in $\text{Na}_2\text{O}-\text{B}_2\text{O}_3-\text{SiO}_2$ glass system. The depolymerization of the glass network proceeds when BO_4 species start to decrease and BO_3 increases conjointly. Therefore, we examined the relationship between the apparent average Q^n derived from Raman spectra, the N_4 value derived from NMR spectra and the Λ_{glass} . We observed a correlation between Q^n , N_4 and Λ_{glass} only for depolymerized glass ($R' > 1$). As Λ_{glass} increases, both Q^n and N_4 decreases (see Table 1). However, for polymerized glasses, N_4 does not show a predictable relationship with Λ_{glass} . More details are presented in the Suppl. Mat.

Another important parameter for characterizing the degree of polymerization in the glass network is the NBO content. We used the ^{11}B NMR and ^{27}Al NMR results to calculate the proportion of NBO in the investigated glasses. The nNBO is calculated with the following equation [63]:

$$\text{nNBO} = \text{nM}^{\text{n}+} - \text{n}^{[4]}\text{B} - \text{n}^{[4]}\text{Al} \quad (2)$$

Where nNBO is the absolute number of NBO, $\text{nM}^{\text{n}+}$ is the absolute number of alkaline or/and alkaline-earth ions, and $\text{n}^{[4]}\text{B}$ and $\text{n}^{[4]}\text{Al}$ is the absolute number of $^{[4]}\text{B}$ and $^{[4]}\text{Al}$ species calculated based on NMR results and glass chemical composition. Numerous studies in the literature also use NMR to analyse the glass structure, allowing us to compare the NBO% ($\text{NBO}\% = \text{nNBO}/\text{nO}$, where nO is the absolute number of oxygen atoms) of our investigated glasses with those from others in the literature. The results are shown in Figure 4 and also provided in Table 1.

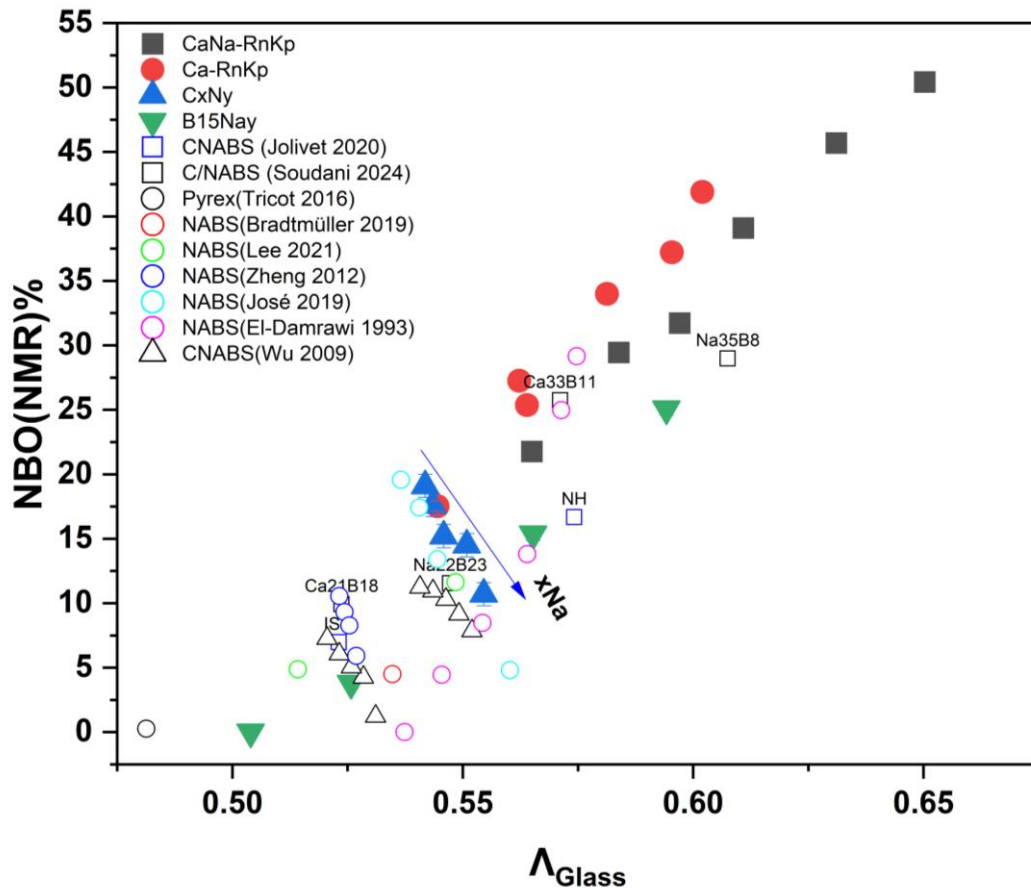


Figure 4. Evolution of NBO content calculated from ^{11}B and ^{27}Al NMR data as function of Λ_{glass} . Solid points represent the investigated glasses in this study, while open points correspond to literature data recalculated using our method. Errors, estimated using the principle of error propagation, are smaller than 1% and are not visible in the figure. The blue arrow indicates the increase of x_{Na} in the CxNy series and series reported in Wu et al., 2009 [41].

The Figure 4 reveals a positive correlation between NBO% and Λ_{glass} not only among our investigated glasses but also in glasses with similar glass systems reported in the literature. As Λ_{glass} increases from 0.48 to 0.65, the NBO% increases from 0 to 50%. Furthermore, three distinct trend lines with a similar slope can be observed: at the top are the $\text{CaO-Al}_2\text{O}_3\text{-B}_2\text{O}_3\text{-SiO}_2$ glasses (e.g. Ca-RnKp series, Ca21B18 and Ca33B11 glasses from Soudani et al. [27]); in the middle are the $\text{CaO-Na}_2\text{O-Al}_2\text{O}_3\text{-B}_2\text{O}_3\text{-SiO}_2$ glasses (e.g. CaNa-RnKp series); and at the bottom are the $\text{Na}_2\text{O-Al}_2\text{O}_3\text{-B}_2\text{O}_3\text{-SiO}_2$ glasses (e.g. B15Nay series, Na22B23, Na35B8, and other $\text{Na}_2\text{O-Al}_2\text{O}_3\text{-B}_2\text{O}_3\text{-SiO}_2$ glasses reported in the literature [27,40,74,75]). This observation suggests that at a given Λ_{glass} value, the $\text{CaO-Al}_2\text{O}_3\text{-B}_2\text{O}_3\text{-SiO}_2$ glasses exhibit a higher NBO% compared to $\text{CaO-Na}_2\text{O-Al}_2\text{O}_3\text{-B}_2\text{O}_3\text{-SiO}_2$ glasses, which in turn have a higher NBO% than $\text{Na}_2\text{O-Al}_2\text{O}_3\text{-B}_2\text{O}_3\text{-SiO}_2$ glasses. For example, when the Λ_{glass} value is 0.6, the NBO% for $\text{CaO-Al}_2\text{O}_3\text{-B}_2\text{O}_3\text{-SiO}_2$, $\text{CaO-Na}_2\text{O-Al}_2\text{O}_3\text{-B}_2\text{O}_3\text{-SiO}_2$ and $\text{Na}_2\text{O-Al}_2\text{O}_3\text{-B}_2\text{O}_3\text{-SiO}_2$ glasses are 37, 32 and 25%, respectively. Additionally, this general observation is also confirmed in the CxNy series and in the two glass series from Wu et al. [41]. As Ca is replaced by Na, which is indicated by the blue arrow, the NBO% decreases witnessing the different behaviour between Na and Ca as well as the MME in glasses. It is noteworthy that the Al/B ratio, also influences the NBO%. Clues can be found in the data from Zheng et al. [42] shown in Figure 4. As B_2O_3 is replaced by Al_2O_3 , Λ_{glass} decreases and NBO% decreases. Given that the Al/B ratio in our investigated glasses is always less than 1, the quantity of $^{51/61}\text{Al}$ is negligible. Thus, glasses with an Al/B ratio greater than 1 reported in the literature were not included in our comparison. These glasses are characterized by a high content of $^{51/61}\text{Al}$, sometimes reaching up to 20% according to the literature, rendering our method for

calculating NBO% no longer suitable because the exact role of ^{[5]/[6]}Al in silicate glasses is still unclear.

It is clear from Figure 4 that the Λ_{glass} is an excellent proxy of the glass degree of polymerization. It should also be pointed out that the Λ_{glass} can be applied to complexed silicate-based glass systems. For instance, the NBO/T defined in early work [76–79] for aluminosilicate glasses and applied to Earth sciences materials cannot be applied to more complex glass compositions such as the aluminoborosilicate glasses investigated in nuclear waste immobilization. The NBO/T only relies on the equilibrium between negative and positive charge within the glass composition and does not take into consideration any potential affinity for one cation or another. For instance, it has been shown that CO₂ dissolution is enhanced in Ca-bearing glasses as compared to Mg-bearing ones [30] suggesting a preferential affinity of CO₂ molecules for Ca²⁺ charge compensating cations. The Λ_{glass} has the advantage to take into consideration the different nature of the cations whether they are network formers or modifiers.

4. Conclusions

In the present work, we used the glass optical basicity (Λ_{glass}) calculated solely from the glass chemical composition, representing the overall chemical environment of oxygen in the glass network. This parameter has been used to investigate the glass network structure. Our study encompassed various aspects of the glass structure, including the local environment of individual atoms as determined by various analytical techniques such as XPS (O 1s binding energy), NMR (chemical shifts of Na and Al), XAS (Ca local environment), and the degree of network polymerization as inferred from NMR-determined NBO content. This work represents the first attempt to use optical basicity as a mean for examining the structure of aluminoborosilicate glass networks on a large sample database.

We established the reliability of Λ_{glass} as a representative of the overall chemical environment of oxygen by demonstrating its strong correlation with the O 1s B.E. obtained from XPS spectra. The recovered trend is in agreement with previous studies. Within the investigated glass system, the higher Λ_{glass} values correspond to lower O 1s B.E., indicating stronger shielding effects and higher oxygen electronegativity. We found that higher Λ_{glass} values were associated with shorter Na-O and Ca-O distances, smaller Al-O-Si bond angles, and increased NBO content. These findings suggest that Λ_{glass} is a powerful indicator of the glass network's structural parameters. Finally, we effectively used Λ_{glass} to study the mixed network modifier effect in glasses. The addition of Ca resulted in a decrease in the Na-O distance, an increase in the symmetry of aluminate tetrahedron, and an increase in the NBO content of the network.

This study underscores the importance of the oxygen chemical environment in understanding the glass network structure. We hope that our findings will provide new insights for future research on glass properties and the optimization of glass formulations. It also points towards the fact that glass optical basicity serves as a reliable parameter to characterize the oxygen environment that 1) can be applied to complex silicate-based glasses and 2) can simulate the glass degree of polymerization that is major structural parameter involved into the incorporation of various element; either volatile species involved in magmatic systems or nuclear waste volatile elements.

Data availability statement

Data of presented results can be provided upon request.

Underlying and related material

Supplementary materials are available at <https://doi.org/10.5281/zenodo.14213087>.

Author contributions

Hanyu Hu: Investigation, Validation, Data curation, Writing – original draft preparation, review & editing.

Sami Soudani: Resources, Writing – review & editing.

Jonathan Hamon: Investigation, Writing – original draft preparation, review & editing.

Nicolas Trcera: Investigation, Writing – original draft preparation, review & editing.

Michael Paris: Supervision, Writing – review & editing.

Yann Morizet: Conceptualization, Methodology, Supervision, Resources, Writing – review & editing.

Competing interests

The authors declare that they have no competing interests.

Acknowledgement

The authors acknowledge the Agence Nationale de la Recherche and Région Pays de la Loire, which financed the current work through the ANR project “Iodine-CLEAN-UP” (Grant No. ANR-20-CE08-0018) and the “Trajectoire nationale de la recherche ligérienne”, respectively. The authors acknowledge the Laboratoire de Planétologie et Géosciences, the Institut des Matériaux de Nantes Jean Rouxel, the Nantes University, and the CNRS for providing access to the analytical facilities. The authors acknowledge SOLEIL for provision of synchrotron radiation facilities and would like to thank LUCIA staff for assistance in using the beamline. The solid-state NMR, XPS and SEM/EDS measurements were performed on IMN’s equipment platform, PLASSMAT, Nantes, France. The authors would like to thank Nicolas Stéphant for the assistance with the SEM/EDS measurements.

References

- (1) Dell, W. J.; Bray, P. J.; Xiao, S. Z. ^{11}B NMR Studies and Structural Modeling of $\text{Na}_2\text{O}-\text{B}_2\text{O}_3-\text{SiO}_2$ Glasses of High Soda Content. *Journal of Non-crystalline Solids* **1983**, *58*, 1–16. [https://doi.org/10.1016/0022-3093\(83\)90097-2](https://doi.org/10.1016/0022-3093(83)90097-2).
- (2) Du, L.-S.; Stebbins, J. F. Network Connectivity in Aluminoborosilicate Glasses: A High-Resolution ^{11}B , ^{27}Al and ^{17}O NMR Study. *Journal of Non-Crystalline Solids* **2005**, *351* (43–45), 3508–3520. <https://doi.org/10.1016/j.jnoncrysol.2005.08.033>.
- (3) Lu, X.; Deng, L.; Du, J.; Vienna, J. D. Predicting Boron Coordination in Multicomponent Borate and Borosilicate Glasses Using Analytical Models and Machine Learning. *Journal of Non-Crystalline Solids* **2021**, *553*, 120490. <https://doi.org/10.1016/j.jnoncrysol.2020.120490>.
- (4) Guggenheim, E. A. The Conceptions of Electrical Potential Difference between Two Phases and the Individual Activities of Ions. *J. Phys. Chem.* **1929**, *33* (6), 842–849. <https://doi.org/10.1021/j150300a003>.
- (5) Susa, M.; Li, F.; Nagata, K. Determination of Refractive Index and Absorption Coefficient of Iron- Oxide-Bearing Slags. *Metall Trans B* **1992**, *23* (3), 331–337. <https://doi.org/10.1007/BF02656289>.
- (6) Moringa, K.; Yoshida, H.; Takebe, H. Compositional Dependence of Absorption Spectra of Ti^{3+} in Silicate, Borate, and Phosphate Glasses. *Journal of the American Ceramic Society* **1994**, *77* (12), 3113–3118. <https://doi.org/10.1111/j.1151-2916.1994.tb04557.x>.
- (7) Duffy, J. A.; Ingram, M. D. Establishment of an Optical Scale for Lewis Basicity in Inorganic Oxyacids, Molten Salts, and Glasses. *J. Am. Chem. Soc.* **1971**, *93* (24), 6448–6454. <https://doi.org/10.1021/ja00753a019>.
- (8) Duffy, J. A.; Ingram, M. D. An Interpretation of Glass Chemistry in Terms of the Optical Basicity Concept. *Journal of Non-Crystalline Solids* **1976**, *21* (3), 373–410. [https://doi.org/10.1016/0022-3093\(76\)90027-2](https://doi.org/10.1016/0022-3093(76)90027-2).
- (9) Nakamura T.; Ueda Y.; Toguri J. M. A New Development of the Optical Basicity. *J. Japan Inst. Metals* **1986**, *50* (5), 456–461. https://doi.org/10.2320/jinstmet1952.50.5_456.
- (10) Duffy, J. A.; Ingram, M. D. Nephelauxetic Effect and Pauling Electronegativity. *J. Chem. Soc., Chem. Commun.* **1973**, No. 17, 635. <https://doi.org/10.1039/c39730000635>.
- (11) Duffy, J. A. Chemical Bonding in the Oxides of the Elements: A New Appraisal. *Journal of Solid State Chemistry* **1986**, *62* (2), 145–157. [https://doi.org/10.1016/0022-4596\(86\)90225-2](https://doi.org/10.1016/0022-4596(86)90225-2).
- (12) Dimitrov, V.; Sakka, S. Electronic Oxide Polarizability and Optical Basicity of Simple Oxides. I. *Journal of Applied Physics* **1996**, *79* (3), 1736–1740. <https://doi.org/10.1063/1.360962>.
- (13) Duffy, J. A. The Refractivity and Optical Basicity of Glass. *Journal of Non-Crystalline Solids* **1986**, *86* (1–2), 149–160. [https://doi.org/10.1016/0022-3093\(86\)90484-9](https://doi.org/10.1016/0022-3093(86)90484-9).
- (14) Iwamoto, N.; Makino, Y.; Kasahara, S. Correlation between Refraction Basicity and Theoretical Optical Basicity Part I. Alkaline and Alkaline-Earth Silicate Glasses. *Journal of Non-Crystalline Solids* **1984**, *68* (2–3), 379–388. [https://doi.org/10.1016/0022-3093\(84\)90018-8](https://doi.org/10.1016/0022-3093(84)90018-8).
- (15) Portier, J.; Campet, G.; Etourneau, J.; Shastry, M. C. R.; Tanguy, B. A Simple Approach to Materials Design: Role Played by an Ionic-Covalent Parameter Based on

- Polarizing Power and Electronegativity. *Journal of Alloys and Compounds* **1994**, 209 (1–2), 59–64. [https://doi.org/10.1016/0925-8388\(94\)91076-6](https://doi.org/10.1016/0925-8388(94)91076-6).
- (16) Leboutellier, A.; Courtine, P. Improvement of a Bulk Optical Basicity Table for Oxidic Systems. *Journal of Solid State Chemistry* **1998**, 137 (1), 94–103. <https://doi.org/10.1006/jssc.1997.7722>.
- (17) Mills, K. C. The Influence of Structure on the Physico-Chemical Properties of Slags. *ISIJ International* **1993**, 33 (1), 148–155. <https://doi.org/10.2355/isijinternational.33.148>.
- (18) Duffy, J. A. Relationship between Optical Basicity and Thermochemistry of Silicates. *J. Phys. Chem. B* **2004**, 108 (23), 7641–7645. <https://doi.org/10.1021/jp031209c>.
- (19) Beckett, J. R. Role of Basicity and Tetrahedral Speciation in Controlling the Thermodynamic Properties of Silicate Liquids, Part 1: The System CaO-MgO-Al₂O₃-SiO₂. *Geochimica et Cosmochimica Acta* **2002**, 66 (1), 93–107. [https://doi.org/10.1016/S0016-7037\(01\)00751-7](https://doi.org/10.1016/S0016-7037(01)00751-7).
- (20) Lenglet, M. Ligand Field Spectroscopy and Chemical Bonding in Cr³⁺-, Fe³⁺-, Co²⁺- and Ni²⁺-Containing Oxidic Solids Influence of the Inductive Effect of the Competing Bonds and Magnetic Interactions on the Degree of Covalency of the 3d M–O Bonds. *Materials Research Bulletin* **2000**, 35 (4), 531–543. [https://doi.org/10.1016/S0025-5408\(00\)00243-9](https://doi.org/10.1016/S0025-5408(00)00243-9).
- (21) Bordes, E. The Role of Structural Chemistry of Selective Catalysts in Heterogeneous Mild Oxidation Catalysis of Hydrocarbons. *Comptes Rendus de l'Académie des Sciences - Series IIC - Chemistry* **2000**, 3 (9), 725–733. [https://doi.org/10.1016/S1387-1609\(00\)01181-6](https://doi.org/10.1016/S1387-1609(00)01181-6).
- (22) Moriceau, P.; Taouk, B.; Bordes, E.; Courtine, P. Correlations between the Optical Basicity of Catalysts and Their Selectivity in Oxidation of Alcohols, Ammoxidation and Combustion of Hydrocarbons. *Catalysis Today* **2000**, 61 (1–4), 197–201. [https://doi.org/10.1016/S0920-5861\(00\)00380-1](https://doi.org/10.1016/S0920-5861(00)00380-1).
- (23) Prakash, B.; Celis, J. P. The Lubricity of Oxides Revised Based on a Polarisability Approach. *Tribol Lett* **2007**, 27 (1), 105–112. <https://doi.org/10.1007/s11249-007-9223-z>.
- (24) Matsumoto, S.; Nanba, T.; Miura, Y. X-Ray Photoelectron Spectroscopy of Alkali Silicate Glasses. *Journal of the Ceramic Society of Japan* **1998**, 106 (1232), 415–421. <https://doi.org/10.2109/jcersj.106.415>.
- (25) Rodriguez, C. P.; McCloy, J. S.; Schweiger, M. J.; Crum, J. V.; Winschell, A. E. *Optical Basicity and Nepheline Crystallization in High Alumina Glasses*; PNNL-20184, EMSP-RPT-003, 1019213; 2011. <http://www.osti.gov/servlets/purl/1019213-ngYFNj/> (accessed 2024-05-16).
- (26) Morizet, Y.; Paris, M.; Hamon, J.; La, C.; Grolleau, S.; Suzuki-Muresan, T. Predicting Iodine Solubility at High Pressure in Borosilicate Nuclear Waste Glasses Using Optical Basicity: An Experimental Study. *J Mater Sci* **2022**, 57 (35), 16600–16618. <https://doi.org/10.1007/s10853-022-07686-8>.
- (27) Soudani, S.; Paris, M.; Morizet, Y. The Effect of Iodine on the Local Environment of Network-Forming Elements in Aluminoborosilicate Glasses: An NMR Study. *Journal of the American Ceramic Society* **2024**, 107 (7), 4557–4571. <https://doi.org/10.1111/jace.19764>.
- (28) Dimitrov, V.; Tasheva, T.; Komatsu, T. Group Optical Basicity and Single Bond Strength of Lead Borate Glasses. *Journal of Chemical Technology and Metallurgy (Print)* **2018**, 53 (6), 1031–1037.

- (29) Morizet, Y.; Brooker, R. A.; Iacono-Marziano, G.; Kjarsgaard, B. A. Quantification of Dissolved CO₂ in Silicate Glasses Using Micro-Raman Spectroscopy. *American Mineralogist* **2013**, *98* (10), 1788–1802. <https://doi.org/10.2138/am.2013.4516>.
- (30) Morizet, Y.; Paris, M.; Sifré, D.; Di Carlo, I.; Gaillard, F. The Effect of Mg Concentration in Silicate Glasses on CO₂ Solubility and Solution Mechanism: Implication for Natural Magmatic Systems. *Geochimica et Cosmochimica Acta* **2017**, *198*, 115–130. <https://doi.org/10.1016/j.gca.2016.11.006>.
- (31) Morizet, Y.; Florian, P.; Paris, M.; Gaillard, F. ¹⁷O NMR Evidence of Free Ionic Clusters Mⁿ⁺ CO₃²⁻ in Silicate Glasses: Precursors for Carbonate-Silicate Liquids Immiscibility. *American Mineralogist* **2017**, *102* (7), 1561–1564. <https://doi.org/doi:10.2138/am-2017-6133>.
- (32) Morizet, Y.; Hamon, J.; La, C.; Jolivet, V.; Suzuki-Muresan, T.; Paris, M. Immobilization of ¹²⁹I in Nuclear Waste Glass Matrixes Synthesized under High-Pressure Conditions: An Experimental Study. *J. Mater. Chem. A* **2021**, *9* (42), 23902–23915. <https://doi.org/10.1039/D1TA05011G>.
- (33) Morizet, Y.; Soudani, S.; Hamon, J.; Paris, M.; La, C.; Gautron, E. Iodine Dissolution Mechanisms in High-Pressure Aluminoborosilicate Glasses and Their Relationship to Oxygen Speciation. *J. Mater. Chem. A* **2023**, *11* (42), 22891–22905. <https://doi.org/10.1039/D3TA05344J>.
- (34) Komatsu, T.; Dimitrov, V.; Tasheva, T.; Honma, T. Electronic Polarizability in Silicate Glasses by Comparison of Experimental and Theoretical Optical Basicities. *Int J of Appl Glass Sci* **2021**, *12* (3), 424–442. <https://doi.org/10.1111/ijag.16009>.
- (35) Nesbitt, H. W.; Bancroft, G. M.; Henderson, G. S.; Ho, R.; Dalby, K. N.; Huang, Y.; Yan, Z. Bridging, Non-Bridging and Free (O²⁻) Oxygen in Na₂O-SiO₂ Glasses: An X-Ray Photoelectron Spectroscopic (XPS) and Nuclear Magnetic Resonance (NMR) Study. *Journal of Non-Crystalline Solids* **2011**, *357* (1), 170–180. <https://doi.org/10.1016/j.jnoncrysol.2010.09.031>.
- (36) Miura, Y.; Kusano, H.; Nanba, T.; Matsumoto, S. X-Ray Photoelectron Spectroscopy of Sodium Borosilicate Glasses. *Journal of Non-Crystalline Solids* **2001**, *290* (1), 1–14. [https://doi.org/10.1016/S0022-3093\(01\)00720-7](https://doi.org/10.1016/S0022-3093(01)00720-7).
- (37) Zajacz, Z. The Effect of Melt Composition on the Partitioning of Oxidized Sulfur between Silicate Melts and Magmatic Volatiles. *Geochimica et Cosmochimica Acta* **2015**, *158*, 223–244. <https://doi.org/10.1016/j.gca.2015.01.036>.
- (38) Moussallam, Y.; Morizet, Y.; Gaillard, F. H₂O–CO₂ Solubility in Low SiO₂-Melts and the Unique Mode of Kimberlite Degassing and Emplacement. *Earth and Planetary Science Letters* **2016**, *447*, 151–160. <https://doi.org/10.1016/j.epsl.2016.04.037>.
- (39) Zajacz, Z.; Tsay, A. An Accurate Model to Predict Sulfur Concentration at Anhydrite Saturation in Silicate Melts. *Geochimica et Cosmochimica Acta* **2019**, *261*, 288–304. <https://doi.org/10.1016/j.gca.2019.07.007>.
- (40) Bradtmüller, H.; Uesbeck, T.; Eckert, H.; Murata, T.; Nakane, S.; Yamazaki, H. Structural Origins of Crack Resistance on Magnesium Aluminoborosilicate Glasses Studied by Solid-State NMR. *J. Phys. Chem. C* **2019**, *123* (24), 14941–14954. <https://doi.org/10.1021/acs.jpcc.9b03600>.
- (41) Wu, J.; Stebbins, J. F. Effects of Cation Field Strength on the Structure of Aluminoborosilicate Glasses: High-Resolution ¹¹B, ²⁷Al and ²³Na MAS NMR. *Journal of Non-Crystalline Solids* **2009**, *355* (9), 556–562. <https://doi.org/10.1016/j.jnoncrysol.2009.01.025>.
- (42) Zheng, Q. J.; Youngman, R. E.; Hogue, C. L.; Mauro, J. C.; Potuzak, M.; Smedskjaer, M. M.; Yue, Y. Z. Structure of Boroaluminosilicate Glasses: Impact of [Al₂O₃]/[SiO₂]

- Ratio on the Structural Role of Sodium. *Phys. Rev. B* **2012**, 86 (5), 054203. <https://doi.org/10.1103/PhysRevB.86.054203>.
- (43) Xue, X.; Stebbins, J. F. ^{23}Na NMR Chemical Shifts and Local Na Coordination Environments in Silicate Crystals, Melts and Glasses. *Physics and Chemistry of Minerals* **1993**, 20, 297–307. <https://doi.org/10.1007/BF00215100>.
- (44) Stebbins, J. Cation Sites in Mixed-Alkali Oxide Glasses: Correlations of NMR Chemical Shift Data with Site Size and Bond Distance. *Solid State Ionics* **1998**, 112 (1–2), 137–141. [https://doi.org/10.1016/S0167-2738\(98\)00224-0](https://doi.org/10.1016/S0167-2738(98)00224-0).
- (45) Lee, S. K.; Stebbins, J. F. The Distribution of Sodium Ions in Aluminosilicate Glasses: A High-Field Na-23 MAS and 3Q MAS NMR Study. *Geochimica et Cosmochimica Acta* **2003**, 67 (9), 1699–1709. [https://doi.org/10.1016/S0016-7037\(03\)00026-7](https://doi.org/10.1016/S0016-7037(03)00026-7).
- (46) George, A. M.; Stebbins, J. F. Dynamics of Na in Sodium Aluminosilicate Glasses and Liquids. *Phys Chem Minerals* **1996**, 23 (8). <https://doi.org/10.1007/BF00242002>.
- (47) Maekawa, H.; Nakao, T.; Shimokawa, S.; Yokokawa, T. Coordination of Sodium Ions in $\text{NaAlO}_2\text{-SiO}_2$ Melts: A High Temperature ^{23}Na NMR Study. *Physics and Chemistry of Minerals* **1997**, 24 (1), 53–65. <https://doi.org/10.1007/s002690050017>.
- (48) Koller, H.; Engelhardt, G.; Kentgens, A. P. M.; Sauer, J. ^{23}Na NMR Spectroscopy of Solids: Interpretation of Quadrupole Interaction Parameters and Chemical Shifts. *J. Phys. Chem.* **1994**, 98 (6), 1544–1551. <https://doi.org/10.1021/j100057a004>.
- (49) Angeli, F.; Delaye, J.; Charpentier, T.; Petit, J.-C.; Ghaleb, D.; Faucon, P. Influence of Glass Chemical Composition on the Na-O Bond Distance: A ^{23}Na 3Q-MAS NMR and Molecular Dynamics Study. *Journal of Non-Crystalline Solids* **2000**, 276 (1), 132–144. [https://doi.org/10.1016/S0022-3093\(00\)00259-3](https://doi.org/10.1016/S0022-3093(00)00259-3).
- (50) Tricot, G. The Structure of Pyrex® Glass Investigated by Correlation NMR Spectroscopy. *Phys. Chem. Chem. Phys.* **2016**, 18 (38), 26764–26770. <https://doi.org/10.1039/C6CP02996E>.
- (51) Dirk Epping, J.; Strojek, W.; Eckert, H. Cation Environments and Spatial Distribution in $\text{Na}_2\text{O-B}_2\text{O}_3$ Glasses: New Results from Solid State NMR. *Phys. Chem. Chem. Phys.* **2005**, 7 (11), 2384. <https://doi.org/10.1039/b502265g>.
- (52) Morizet, Y.; Trcera, N.; Larre, C.; Rivoal, M.; Le Menn, E.; Vantelon, D.; Gaillard, F. X-Ray Absorption Spectroscopic Investigation of the Ca and Mg Environments in CO_2 -Bearing Silicate Glasses. *Chemical Geology* **2019**, 510, 91–102. <https://doi.org/10.1016/j.chemgeo.2019.02.014>.
- (53) Binsted, N.; Greaves, G. N.; Henderson, C. M. B. An EXAFS Study of Glassy and Crystalline Phases of Compositions $\text{CaAl}_2\text{Si}_2\text{O}_8$ (Anorthite) and $\text{CaMgSi}_2\text{O}_6$ (Diopside). *Contributions to Mineralogy and Petrology* **1985**, 89 (2), 103–109. <https://doi.org/10.1007/BF00379446>.
- (54) Le Cornec, D.; Cormier, L.; Galois, L.; Baptiste, B.; Trcera, N.; Izoret, L.; Calas, G. Molecular Structure of Amorphous Slags: An Experimental and Numerical Approach. *Journal of Non-Crystalline Solids* **2021**, 556, 120444. <https://doi.org/10.1016/j.jnoncrysol.2020.120444>.
- (55) Taniguchi, T.; Okuno, M.; Matsumoto, T. X-Ray Diffraction and EXAFS Studies of Silicate Glasses Containing Mg, Ca and Ba Atoms. *Journal of Non-Crystalline Solids* **1997**, 211 (1–2), 56–63. [https://doi.org/10.1016/S0022-3093\(96\)00632-1](https://doi.org/10.1016/S0022-3093(96)00632-1).
- (56) Hannon, A. C.; Parker, J. M. The Structure of Aluminate Glasses by Neutron Diffraction. *Journal of Non-Crystalline Solids* **2000**, 274 (1), 102–109. [https://doi.org/10.1016/S0022-3093\(00\)00208-8](https://doi.org/10.1016/S0022-3093(00)00208-8).

- (57) Cormier, L.; Calas, G.; Beuneu, B. Structural Changes between Soda-Lime Silicate Glass and Melt. *Journal of Non-Crystalline Solids* **2011**, 357 (3), 926–931. <https://doi.org/10.1016/j.jnoncrysol.2010.10.014>.
- (58) Cormier, L.; Ghaleb, D.; Neuville, D. R.; Delaye, J.-M.; Calas, G. Chemical Dependence of Network Topology of Calcium Aluminosilicate Glasses: A Computer Simulation Study. *Journal of Non-Crystalline Solids* **2003**, 332 (1–3), 255–270. <https://doi.org/10.1016/j.jnoncrysol.2003.09.012>.
- (59) Gambuzzi, E.; Pedone, A.; Menziani, M. C.; Angeli, F.; Florian, P.; Charpentier, T. Calcium Environment in Silicate and Aluminosilicate Glasses Probed by ^{43}Ca MQMAS NMR Experiments and MD-GIPAW Calculations. *Solid State Nuclear Magnetic Resonance* **2015**, 68–69, 31–36. <https://doi.org/10.1016/j.ssnmr.2015.04.003>.
- (60) Shimoda, K.; Tobu, Y.; Shimoikeda, Y.; Nemoto, T.; Saito, K. Multiple Ca^{2+} Environments in Silicate Glasses by High-Resolution ^{43}Ca MQMAS NMR Technique at High and Ultra-High (21.8T) Magnetic Fields. *Journal of Magnetic Resonance* **2007**, 186 (1), 156–159. <https://doi.org/10.1016/j.jmr.2007.01.019>.
- (61) Gambuzzi, E.; Pedone, A.; Menziani, M. C.; Angeli, F.; Caurant, D.; Charpentier, T. Probing Silicon and Aluminium Chemical Environments in Silicate and Aluminosilicate Glasses by Solid State NMR Spectroscopy and Accurate First-Principles Calculations. *Geochimica et Cosmochimica Acta* **2014**, 125, 170–185. <https://doi.org/10.1016/j.gca.2013.10.025>.
- (62) Jolivet, V.; Morizet, Y.; Paris, M.; Suzuki-Muresan, T. High Pressure Experimental Study on Iodine Solution Mechanisms in Nuclear Waste Glasses. *Journal of Nuclear Materials* **2020**, 533, 152112. <https://doi.org/10.1016/j.jnucmat.2020.152112>.
- (63) Soudani, S.; Paris, M.; Morizet, Y. Influence of High-Pressure on the Short-Range Structure of Ca or Na Aluminoborosilicate Glasses from ^{11}B and ^{27}Al Solid-State NMR. *Journal of Non-Crystalline Solids* **2024**, 638, 123085. <https://doi.org/10.1016/j.jnoncrysol.2024.123085>.
- (64) Lee, A. C.; Lee, S. K. Effect of Composition on Structural Evolution and NMR Parameters of Quadrupolar Nuclides in Sodium Borate and Aluminoborosilicate Glasses: A View from High-Resolution ^{11}B , ^{27}Al , and ^{17}O Solid-State NMR. *Journal of Non-Crystalline Solids* **2021**, 555, 120271. <https://doi.org/10.1016/j.jnoncrysol.2020.120271>.
- (65) Merzbacher, C. I.; Sherriff, B. L.; Hartman, J. S.; White, W. B. A High-Resolution ^{29}Si and ^{27}Al NMR Study of Alkaline Earth Aluminosilicate Glasses. *Journal of Non-Crystalline Solids* **1990**, 124 (2), 194–206. [https://doi.org/10.1016/0022-3093\(90\)90263-L](https://doi.org/10.1016/0022-3093(90)90263-L).
- (66) Neuville, D. R.; Cormier, L.; Massiot, D. Al Coordination and Speciation in Calcium Aluminosilicate Glasses: Effects of Composition Determined by ^{27}Al MQ-MAS NMR and Raman Spectroscopy. *Chemical Geology* **2006**, 229 (1), 173–185. <https://doi.org/10.1016/j.chemgeo.2006.01.019>.
- (67) Kohn, S. C.; Henderson, C. M.; Dupree, R. Si-Al Ordering in Leucite Group Minerals and Ion-Exchanged Analogues; an MAS NMR Study. *American Mineralogist* **1997**, 82 (11–12), 1133–1140. <https://doi.org/10.2138/am-1997-11-1211>.
- (68) Lippmaa, E.; Samoson, A.; Magi, M. High-Resolution Aluminum-27 NMR of Aluminosilicates. *J. Am. Chem. Soc.* **1986**, 108 (8), 1730–1735. <https://doi.org/10.1021/ja00268a002>.
- (69) Phillips, B. L.; Kirkpatrick, R. J.; Putnis, A. Si,Al Ordering in Leucite by High-Resolution ^{27}Al MAS NMR Spectroscopy. *Physics and Chemistry of Minerals* **1989**, 16 (6), 591–598. <https://doi.org/10.1007/BF00202216>.

- (70) Baltisberger, J. H.; Xu, Z.; Stebbins, J. F.; Wang, S. H.; Pines, A. Triple-Quantum Two-Dimensional ^{27}Al Magic-Angle Spinning Nuclear Magnetic Resonance Spectroscopic Study of Aluminosilicate and Aluminate Crystals and Glasses. *J. Am. Chem. Soc.* **1996**, *118* (30), 7209–7214. <https://doi.org/10.1021/ja9606586>.
- (71) Lee, S. K.; Stebbins, J. F. The Structure of Aluminosilicate Glasses: High-Resolution ^{17}O and ^{27}Al MAS and 3QMAS NMR Study. *J. Phys. Chem. B* **2000**, *104* (17), 4091–4100. <https://doi.org/10.1021/jp994273w>.
- (72) Angeli, F.; Delaye, J.; Charpentier, T.; Petit, J.-C.; Ghaleb, D.; Faucon, P. Investigation of Al–O–Si Bond Angle in Glass by ^{27}Al 3Q-MAS NMR and Molecular Dynamics. *Chemical Physics Letters* **2000**, *320* (5), 681–687. [https://doi.org/10.1016/S0009-2614\(00\)00277-3](https://doi.org/10.1016/S0009-2614(00)00277-3).
- (73) Quintas, A.; Caurant, D.; Majérus, O.; Loiseau, P.; Charpentier, T.; Dussossoy, J.-L. ZrO_2 Addition in Soda-Lime Aluminoborosilicate Glasses Containing Rare Earths: Impact on the Network Structure. *Journal of Alloys and Compounds* **2017**, *714*, 47–62. <https://doi.org/10.1016/j.jallcom.2017.04.182>.
- (74) El-Damrawi, G.; Müller-Warmuth, W.; Doweidar, H.; Gohar, I. A. Structure and Heat Treatment Effects of Sodium Borosilicate Glasses as Studied by ^{29}Si and ^{11}B NMR. *Journal of Non-Crystalline Solids* **1992**, *146*, 137–144. [https://doi.org/10.1016/S0022-3093\(05\)80485-5](https://doi.org/10.1016/S0022-3093(05)80485-5).
- (75) Marcial, J.; Saleh, M.; Watson, D.; Martin, S. W.; Crawford, C. L.; McCloy, J. S. Boron-Speciation and Aluminosilicate Crystallization in Alkali Boroaluminosilicate Glasses along the $\text{NaAl}_{1-x}\text{B}_x\text{SiO}_4$ and $\text{LiAl}_{1-x}\text{B}_x\text{SiO}_4$ Joins. *Journal of Non-Crystalline Solids* **2019**, *506*, 58–67. <https://doi.org/10.1016/j.jnoncrysol.2019.01.001>.
- (76) Mysen, B. O.; Virgo, D.; Seifert, F. A. The Structure of Silicate Melts: Implications for Chemical and Physical Properties of Natural Magma. *Reviews of Geophysics* **1982**, *20* (3), 353–383. <https://doi.org/10.1029/RG020i003p00353>.
- (77) Kuryaeva, R. G. Degree of Polymerization of the $\text{CaAl}_2\text{Si}_2\text{O}_8$ Aluminosilicate Glass. *Glass Phys Chem* **2006**, *32* (5), 505–510. <https://doi.org/10.1134/S1087659606050026>.
- (78) Bechgaard, T. K.; Goel, A.; Youngman, R. E.; Mauro, J. C.; Rzoska, S. J.; Bockowski, M.; Jensen, L. R.; Smedskjaer, M. M. Structure and Mechanical Properties of Compressed Sodium Aluminosilicate Glasses: Role of Non-Bridging Oxygens. *Journal of Non-Crystalline Solids* **2016**, *441*, 49–57. <https://doi.org/10.1016/j.jnoncrysol.2016.03.011>.
- (79) Le Losq, C.; Mysen, B. O.; Cody, G. D. Water Solution Mechanism in Calcium Aluminosilicate Glasses and Melts: Insights from in and Ex Situ Raman and ^{29}Si NMR Spectroscopy. *Comptes Rendus. Géoscience* **2022**, *354* (S1), 199–225. <https://doi.org/10.5802/crgeos.127>.